Available online at www.sciencedirect.com
SCIENCE DIRECT®
Chemical Physics Letters 392 (2004) 486–492
CHEMICAL PHYSICS LETTERS
www.elsevier.com/locate/cplett

Quantum monodromy for diatomic molecules in combined electrostatic and pulsed nonresonant laser fields

Carlos A. Arango, William W. Kennerly, Gregory S. Ezra *

Baker Laboratory, Department of Chemistry and Chemical Biology, Cornell University, Ithaca NY 14853, USA

Received 21 April 2004; in final form 25 May 2004
Available online 19 June 2004

Abstract

We investigate the classical and quantum mechanics of diatomic molecules in combined electrostatic and pulsed laser fields. The integrable case of collinear static and linearly polarized laser fields exhibits both classical and quantum monodromy, and energy–momentum diagrams are presented for several physically relevant field combinations. Although the tilted field problem is nonintegrable, a quantum $\langle \hat{H} \rangle : \sqrt{\langle m^2 \rangle}$ lattice for eigenstates retains much of the structure of the integrable limit and is organized by classical periodic orbits. The regular structure of the quantum lattice in the integrable limit is disrupted in an energy range associated with the onset of chaotic classical motion.

1. Introduction

A rigid polar diatomic molecule interacting with a static electric field is the molecular realization of the venerable spherical pendulum problem [1]. It has been known for some time that the classical spherical pendulum, although an integrable system [2], exhibits the phenomenon of *monodromy*; that is, a topological obstruction to the existence of a global set of action-angle variables [1,3]. The quantum spherical pendulum exhibits *quantum monodromy* [4]. The presence of quantum monodromy is manifest as an apparent defect in the discrete lattice of states constituting the quantum energy–momentum diagram [4]. Parallel transport of a lattice cell around a circuit enclosing the defect results in a nontrivial unimodular transformation of the lattice cell described by a monodromy matrix M [5]. Quantum monodromy has been observed in the spherical pendulum [4,6], champagne bottle potential [7], hydrogen atom in crossed fields [8], quasilinear molecules [6,9–11], and symmetric and quasisymmetric tops in a static electric field [12].

Polar diatomics and symmetric rotors in intense electrostatic fields have been studied in the production of oriented (pendular [13–15]) states by 'brute force' methods [16]. If, in addition, the molecules are subject to collinear pulsed nonresonant laser fields, a significant degree of orientation can be achieved with weaker static fields than those required for brute-force orientation [17,18].

Nonpolar molecules with anisotropic polarizabilities subject to nonresonant laser pulses exhibit alignment [1] whose time-dependence depends on the length of the pulse compared to the rotational period [19–23]. In this Letter, we consider a polar diatomic with anisotropic polarizability subject to both electrostatic and pulsed nonresonant laser fields in the (experimentally accessible [24,25]) adiabatic regime. We therefore, study instantaneous eigenstates of the molecule-field system.

For collinear static and linearly polarized laser fields, the component of angular momentum along the field direction is conserved and the problem is integrable. This integrable system exhibits monodromy [3] for

* Corresponding author. Fax: +6072554137.
E-mail address: gse1@cornell.edu (G.S. Ezra).

[1] Orientation $\equiv \langle P_1(\cos\theta) \rangle$, averaged over the rotational distribution function. Alignment $\equiv \langle P_2(\cos\theta) \rangle$. The angle θ describes the direction of a molecule-fixed axis with respect to the static external field direction.

0009-2614/$ - see front matter © 2004 Elsevier B.V. All rights reserved.
doi:10.1016/j.cplett.2004.06.002

nonzero static field strength. For physically reasonable values of molecular parameters, the diatomic in combined collinear fields provides a realization of the spherical pendulum plus quadratic potential model. The classical energy–momentum diagram then consists of two regions (leaves) 'glued' together along a critical cut [10], where the size and shape of the overlap region of the leaves can be changed by tuning the values of the field strengths. The quantum state lattice exhibits corresponding quantum monodromy, and the classical relative equilibria [26,27] organize the quantum lattice structure. For a diatomic subject to a static field perpendicular to a circularly polarized laser pulse, the classical energy–momentum diagram exhibits a pair of isolated critical points of the energy–momentum map.

If the fields are not collinear but are *tilted* with respect to one another, then there is no longer a conserved component of angular momentum, and the corresponding classical dynamical system is nonintegrable. For large tilting angles, $\beta \sim \pi/4$, there is extensive classical chaos. (The classical phase space structure is discussed elsewhere [28].) For small tilting angles, even though the problem is formally nonintegrable, much of the structure of the quantum state lattice in the integrable case persists when the fields are tilted. The primary periodic orbits, which undergo extensive bifurcations in the tilted field case, now serve to organize the global phase space structure [29] (cf. the discussion of the quasisymmetric top case given by Kozin and Roberts [12]).

2. Hamiltonian for diatomic in external fields

A rigid polar diatomic in a static electric field ε_S along the space-fixed z-axis is described by the spherical pendulum Hamiltonian

$$H = \frac{j^2}{2I} - \varepsilon_S D\cos\theta = \frac{1}{2I}\left[p_\theta^2 + \frac{p_\phi^2}{\sin^2\theta}\right] - \varepsilon_S D\cos\theta, \quad (1)$$

where D is the magnitude of the dipole moment, I is the moment of inertia, spherical polar coordinates (θ,ϕ) specify the orientation of the rotor axis, and (p_θ, p_ϕ) are conjugate momenta. The angle between the diatom axis and the external field is θ. Although the total angular momentum j of the rotor is not conserved, the z-component m (p_ϕ) is a constant of the motion.

The time-averaged Hamiltonian for a diatomic in a rapidly oscillating (infrared frequency), nonresonant linearly polarized laser field $\varepsilon_L(t)$ along the z-axis is [19]

$$H = \frac{j^2}{2I} - \frac{\langle \varepsilon_L(t)^2\rangle}{2}\left[\alpha_\perp + (\alpha_\parallel - \alpha_\perp)\cos^2\theta\right], \quad (2)$$

where $\alpha_\parallel$, $\alpha_\perp$ are components of the polarizability tensor parallel and perpendicular to the diatomic axis, respectively, and $\langle \varepsilon_L(t)^2\rangle$ denotes the time-averaged laser field. If $\varepsilon_L(t) = f(t)\varepsilon_L\cos(2\pi\nu t)$, where ν is the laser frequency, ε_L the field amplitude, and $f(t)$ a slowly varying envelope function, then $\langle \varepsilon_L(t)^2\rangle = f^2\varepsilon_L^2/2$. Note that the molecule-field interaction depends on $\cos^2\theta$ and that, for a diatomic, $\alpha_\parallel - \alpha_\perp > 0$. The projection m is again a constant of the motion, and the effective potential in the orientation angle θ has a double minimum for $m = 0$. Quantum mechanically, for a strong laser field, extensive j-mixing occurs to produce aligned rather than oriented states [18,20,30]; the symmetric double well potential leads to the appearance of closely spaced doublets [18]. Conservation of m implies that the classical system is integrable.

A more complicated but still integrable problem results when *collinear* static and laser fields are applied [18]. In terms of dimensionless variables $\omega \equiv \varepsilon_S D/B$ and $\Delta\omega \equiv \langle \varepsilon_L(t)^2\rangle(\alpha_\parallel - \alpha_\perp)/2B$ ($B \equiv \hbar^2/2I$), and omitting a constant energy shift, the scaled Hamiltonian $\tilde{H} \equiv H/B$ is

$$\tilde{H} = j^2 - \omega\cos\theta - \Delta\omega\cos^2\theta, \quad (3)$$

where $\omega\cos\theta$ is the static field term, $\Delta\omega\cos^2\theta$ is the term due to the laser field, and j is now a dimensionless angular momentum measured in units of $\hbar$. For $\omega < 2\Delta\omega$, $m = 0$, the effective potential in θ has the form of an asymmetric double well [18], while for $\omega \geqslant 2\Delta\omega$ there is only a single minimum. The number of aligned states trapped in the double well increases as the parameter $\Delta\omega$ increases, and the potential is more asymmetric for larger ω. The classical dynamics depends only on the dimensionless ratio $\mathscr{A} \equiv \omega/\Delta\omega$, whereas the quantum problem depends also on the magnitude of $\hbar$ through the rotational energy $B\hbar^2$.

If the diatomic is subject to a static field along the z-axis together with a pulsed laser field circularly polarized in the xy-plane, with field $\varepsilon_L(t) = f(t)\varepsilon_L(\cos\Omega t, \sin\Omega t, 0)$, the scaled Hamiltonian has the form (3) with $\Delta\omega$ negative. Molecules therefore tend to align in the xy-plane.

Now consider the case when the static and linearly polarized laser field directions are *tilted* with respect to one another [17,18,28]. Setting the static field ε_S along the direction $(\sin\beta, 0, \cos\beta)$ in the xz-plane, the scaled classical Hamiltonian is

$$\tilde{H}(\theta,\phi,p_\theta,p_\phi) = \left[p_\theta^2 + \frac{p_\phi^2}{\sin^2\theta}\right] - \omega(\sin\beta\sin\theta\cos\phi + \cos\beta\cos\theta) - \Delta\omega\cos^2\theta. \quad (4)$$

The scaled Hamiltonian (4) no longer conserves m and is classically nonintegrable [28]. The onset of chaotic classical motion is a consequence of a competition between the tendency for the diatomic to align along the laser field axis and the tendency to orient along the static field.

Quantum mechanical eigenvalues and eigenvectors for Hamiltonians (1)–(4) are obtained by matrix diagonalization in a basis of spherical harmonics $Y_M^J(\theta,\phi)$.

Our computer program allows for nonconservation of the quantum number M, as required for the tilted fields case. All potentials considered here are invariant under the coordinate transformation $(\theta,\phi)\mapsto(\theta,-\phi)$, and a suitable symmetrized basis is:

$$|J,|M|,\pm\rangle \equiv \frac{1}{\sqrt{2}}\left[Y^J_{|M|} \pm (-)^M Y^J_{-|M|}\right], \quad 1 \leqslant |M| \leqslant J, \tag{5}$$

with $|J,0,+\rangle \equiv Y^J_{M=0}$.

The model parameters we use are appropriate for the diatomic KCl (cf. Table 3 of [18]): $B = 0.1286$ cm^{-1}, $\mu = 10.48$ D, $\Delta\alpha \simeq 3.1$ Å^3, so that $\omega = 60$ for $\varepsilon_S = 44$ kV cm^{-1} and $\Delta\omega = 240$ for $\varepsilon_L = 10^{12}$ W cm^{-2}. For KCl we therefore have $\Delta\omega \lesssim 240$ and $\omega \lesssim 60$ for experimentally attainable field strengths, so that the number of trapped pendular states created by both the static field and the laser pulse for reasonable intensities is large enough for semiclassical considerations to be appropriate ($\omega, \Delta\omega \gg 1$). The ratio of the static field interaction energy to the laser field interaction energy $\mathscr{A}$ can moreover be in the range 1/6–1/3, where significant classical chaos is present for large tilt angles [28].

3. Classical and quantum monodromy: collinear fields

For both the classical and quantum mechanical collinear fields problem, the z-component of angular momentum m is a constant of the motion. Classical relative equilibria [26] are critical points of the effective potential:

$$V_{\text{eff}}(\theta;m) = \frac{m^2}{\sin^2\theta} - \omega\cos\theta - \Delta\omega\cos^2\theta, \tag{6}$$

$\partial V_{\text{eff}}/\partial\theta = 0$. Relative equilibria are shown in the bifurcation diagram Fig. 1a, which plots E versus θ for $\mathscr{A} = (1/3)$, $\beta = 0$. The two stable relative equilibria are shown as thick solid lines and the unstable relative equilibrium by a thick dashed line. The lowest energy point on each of these three curves is a relative equilibrium with $m = 0$. The two stable relative equilibria with $m = 0$ correspond to the rotor either parallel ($\theta = 0$) or antiparallel ($\theta = \pi$) to the field; the unstable relative equilibrium corresponds to a one-parameter family of stationary rotor configurations in the full phase space, parameterized by azimuthal angle $\phi = \phi_0$. For $|m| > 0$, the relative equilibria are associated with pairs of periodic orbits with $\pm m$ (conical pendulum orbits [31]). At higher energies, one of the stable relative equilibrium periodic orbit pairs merges with the unstable relative equilibrium orbit pair in a pair of saddle-node bifurcations [32]. In addition to the relative equilibria, there also exist one-parameter families of planar periodic orbits passing through the poles. These orbits are librational (pendular) for energies below the barrier height, and rotational at higher energies. The transition from librational to rotational motion occurs at precisely the energy at which the unstable relative equilibrium appears.

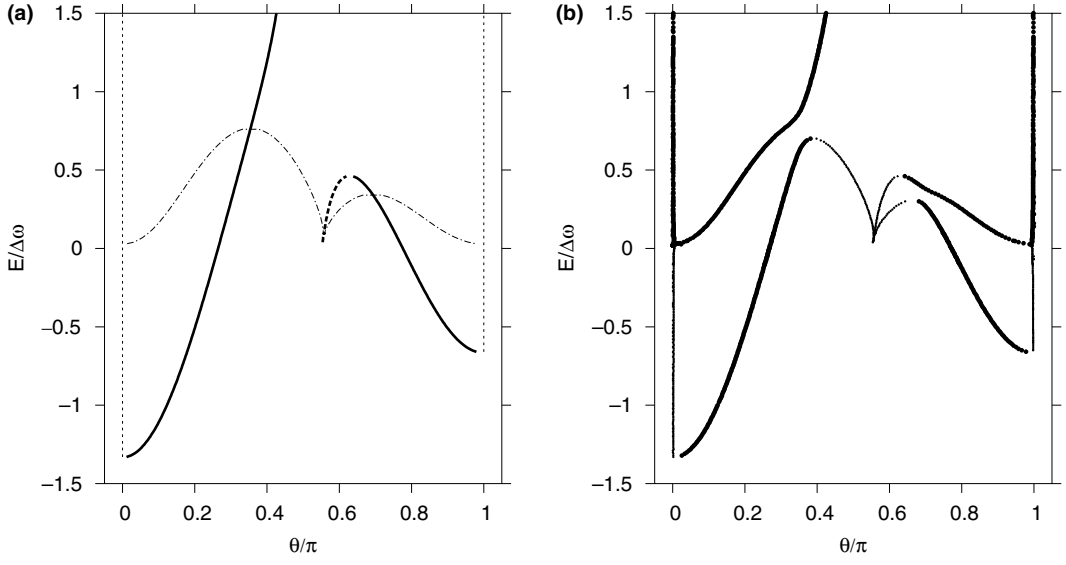

Fig. 1. Energy $E/\Delta\omega$ versus polar angle θ for relative equilibria and periodic orbits of a rotor in static plus linearly polarized laser fields, $\omega/\Delta\omega = (1/3)$. (a) Collinear fields (tilt angle $\beta = 0$), integrable case. Angular momentum component m is a constant of the motion for each orbit. Relative equilibria (critical points of the effective potential (6)) are shown together with 1:1 resonant periodic orbits bifurcating from them. Stable relative equilibria are shown as thick solid lines, the unstable relative equilibrium by a thick dashed line, and marginally stable resonant periodic orbits by dash-dot lines. Parabolic polar orbits with $p_\phi = 0$ are denoted by dashed lines at $\theta = 0$ and $\theta = \pi$. (b) Tilted fields (tilt angle $\beta = \pi/100$), nonintegrable case. Angular momentum component m is not a constant of the motion. Periodic orbits evolving from the relative equilibria and periodic orbits of (a) are shown. Stable periodic orbits are denoted by thick lines, unstable periodic orbits by thinner lines.

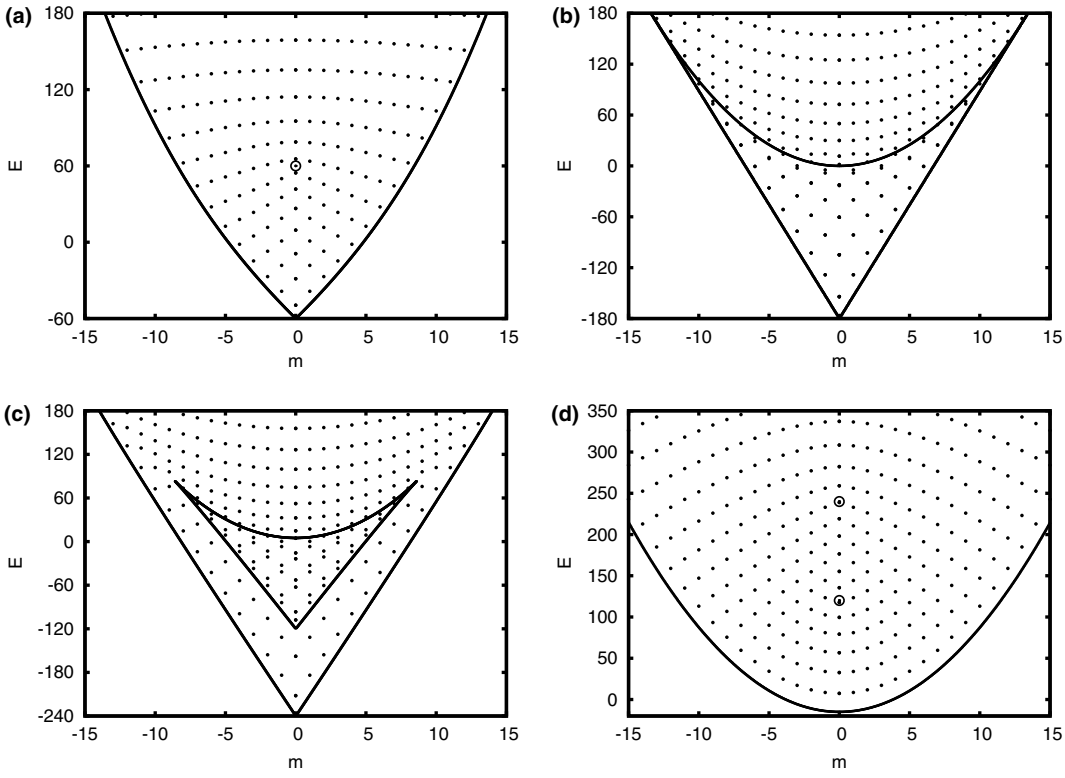

Fig. 2. Classical energy momentum diagrams (E versus m) plotted together with corresponding quantum $E : m$ lattices for four field combinations. Quantum states are denoted by filled circles, classical relative equilibria by solid lines and open circles. (a) Static field only (spherical pendulum): $\omega = 60, \Delta\omega = 0$ (cf. Eq. (3)). (b) Linearly polarized laser field only: $\omega = 0$, $\Delta\omega = +180$. (c) Collinear field case: $\omega = 60$, $\Delta\omega = +180$. (d) Static field along the z-axis combined with circularly polarized laser pulse in the xy-plane: $\omega = 60$, $\Delta\omega = -180$.

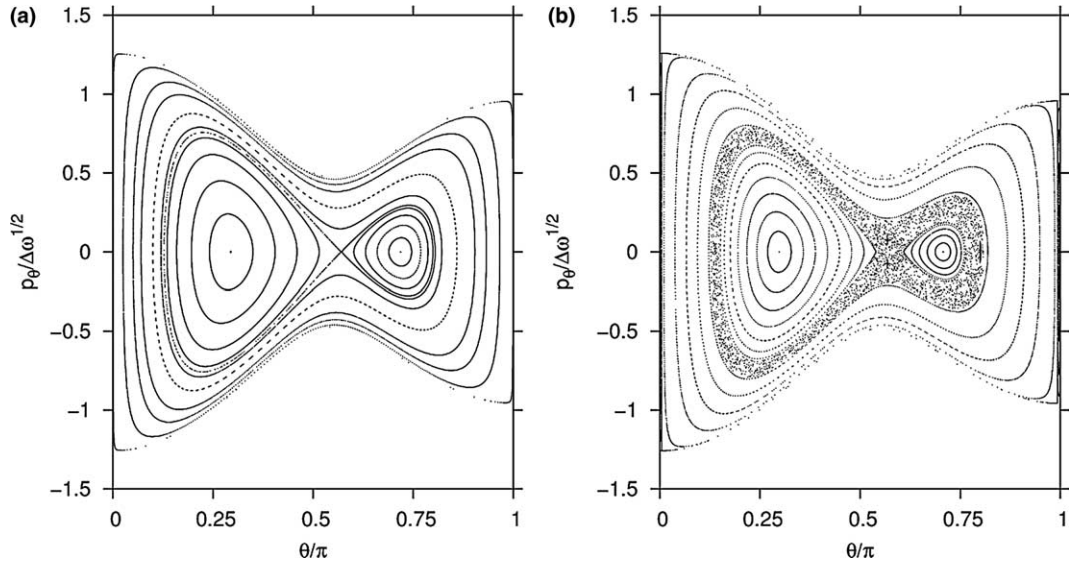

Fig. 3. (θ, p_θ) surfaces of section are plotted for the rotor in static plus linearly polarized laser fields. The sectioning condition is $\phi = 0$, $\dot{\phi} > 0$. Parameter values are: $\omega/\Delta\omega = (1/3)$, $E/\Delta\omega = +0.25$. (a) Collinear fields (tilt angle $\beta = 0$); integrable case. (b) Tilted fields (tilt angle $\beta = \pi/100$); nonintegrable case.

Also shown are 1:1 resonant parabolic (neutrally stable) periodic orbits that emerge from the planar polar orbits and merge with the relative equilibria (conical pendulum orbits) at higher energy. These resonant periodic orbits occur in one-parameter families, with each family filling a rational torus. Particular orbits in the

family are found by iteration of the symmetry line $p_\theta = 0$ on the $\phi = 0$, $\dot{\phi} > 0$ surface of section [28,33]. The thin lines in Fig. 1a show the θ values for 1:1 resonant periodic orbits on the symmetry line at energy E. Each resonant torus intersects the symmetry line at two points, one on each side of a stable relative equilibrium. Unlike the periodic orbits associated with the relative equilibria, the angle θ is not constant along the 1:1 resonant periodic orbits.

The corresponding E versus m plot for the relative equilibria is the classical energy–momentum diagram [1]. Energy–momentum diagrams are shown for four field combinations in Fig. 2. Fig. 2a shows the case $\omega = 60, \Delta\omega = 0$, which corresponds to static field only (the spherical pendulum). The quantum state lattice in this case exhibits a defect located at the point $E = 60, m = 0$, which is the location of the isolated unstable classical relative equilibrium. It is readily verified that the quantum monodromy matrix is $M = \begin{bmatrix} 1 & 0 \\ 1 & 1 \end{bmatrix}$ [4]. Fig. 2b shows the energy momentum diagram for the linearly polarized laser field only: $\Delta\omega = 180$, $\mathscr{A} = 0$. The effective potential in this case is a symmetric double well for $m = 0$, and there is no monodromy (cf. Fig. 3 of [8]). The quantum state lattice is divided into two regions associated with below-barrier and above-barrier states, respectively. Fig. 2c shows the collinear field case with $\Delta\omega = 180$, $\mathscr{A} = 1/3$. Application of the combined laser and static fields results in a triangular region in which the two leaves of the energy–momentum diagram overlap. The size of the overlap region can be altered by tuning the field strengths. The quantum monodromy matrix for parallel transport of a lattice cell around the critical cut at the top of the overlap region is the same as for the spherical pendulum example. The triangular region is the portion of the $E : m$ diagram in which trapped pendular states exist on both sides of the asymmetric double well effective potential (6).

Finally, in Fig. 2d we take $\omega = 60$, $\Delta\omega = -180$, corresponding to a diatomic in combined static field along the z-axis and circularly polarized pulse in the xy-plane. Note the characteristic quadratic dependence of the energy of the stable relative equilibrium on the angular momentum component m. For $m = 0$, the effective potential $V(\theta)$ has stationary points at $\theta \sim \pi/2$ (minimum) and $\theta = 0, \pi$ (maxima). The maxima are at different energies when $\omega \neq 0$, and disappear for $m \neq 0$. There are therefore two distinct isolated unstable relative equilibria on the $m = 0$ line, which give rise to defects in the quantum state lattice. The monodromy matrix for transport of a lattice cell around a circuit enclosing both defects is found to be $M = \begin{bmatrix} 1 & 0 \\ 2 & 1 \end{bmatrix}$, and is different from the spherical pendulum case (see [1], p. 386; also [34]).

4. Tilted fields: nonintegrable case

As already mentioned, the classical problem is nonintegrable for the tilted static field-linearly polarized laser field case ($\beta \neq 0$) [28]. We consider here small values of the tilting angle, $\beta = \pi/100$ and $\pi/20$. A (θ, p_θ) surface of section, defined by the sectioning condition $\phi = 0$, $\dot{\phi} > 0$, is shown in Fig. 3b ($E/\Delta\omega = +0.25$, $\mathscr{A} = 1/3$), and illustrates the onset of localized chaotic motion in the tilted field case even for $\beta = \pi/100$.

The corresponding primary periodic orbit bifurcation diagram for tilted fields is given in Fig. 1b. Stable orbits are represented by thick lines and unstable orbits by thin lines. In contrast to the relative equilibria of Fig. 1a, the polar angle θ is not constant along any of the orbits shown in Fig. 1b. Three unstable periodic orbit pairs now appear at an energy corresponding to the top of the (ϕ-dependent) potential barrier, and each of these unstable orbits merges with a stable periodic orbit at higher energy in a saddle-node bifurcation. Each one-parameter family of marginally stable resonant periodic orbits is replaced by a stable/unstable pair of periodic orbits. Similarly, the one-parameter family of periodic orbits at the poles becomes a pair of periodic orbits in the nonintegrable case. It is clear from Fig. 1 that knowledge of both the relative equilibria and low order resonant periodic orbits in the integrable limit is needed to understand the structure of the bifurcation diagram for tilted fields.

As m is no longer a conserved quantity/good quantum number, there would in general appear to be no useful construction analogous to the energy–momentum plot. Nevertheless, for small tilt angles we find that a plot of E versus $(\overline{m^2})^{1/2}$ (the square root of the time-average of p_ϕ^2) for the classical periodic orbits yields a diagram very similar in appearance to the classical $E : |m|$ diagram in the integrable case. Moreover, a corresponding quantum state lattice can be defined by plotting energy eigenvalue E_j versus $\sqrt{\langle \hat{m}^2 \rangle_j}$ for each eigenstate j of the tilted field problem. (For a similar approach applied to coupled spin systems, see [35].) Classical and quantum $E : \sqrt{\langle m^2 \rangle}$ plots for $\Delta\omega = 180$, $\mathscr{A} = 1/3$ are shown in Fig. 4a ($\beta = 0$) and Fig. 4b ($\beta = \pi/100$). Positive parity eigenstates are plotted. Fig. 4a is identical with one half of Fig. 2c, except for the addition of the $E : |m|$ curve for 1:1 resonant periodic orbits. From Fig. 4b it is apparent that much of the structure of the lattice from the integrable limit persists for small tilting angles. In particular, the region associated with the existence of bound states in both wells is still readily identifiable in the tilted fields case. The regular quantum lattice structure of the integrable limit is however, noticeably disrupted in the energy range in which classically chaotic phase space structure appears (cf. [35]).

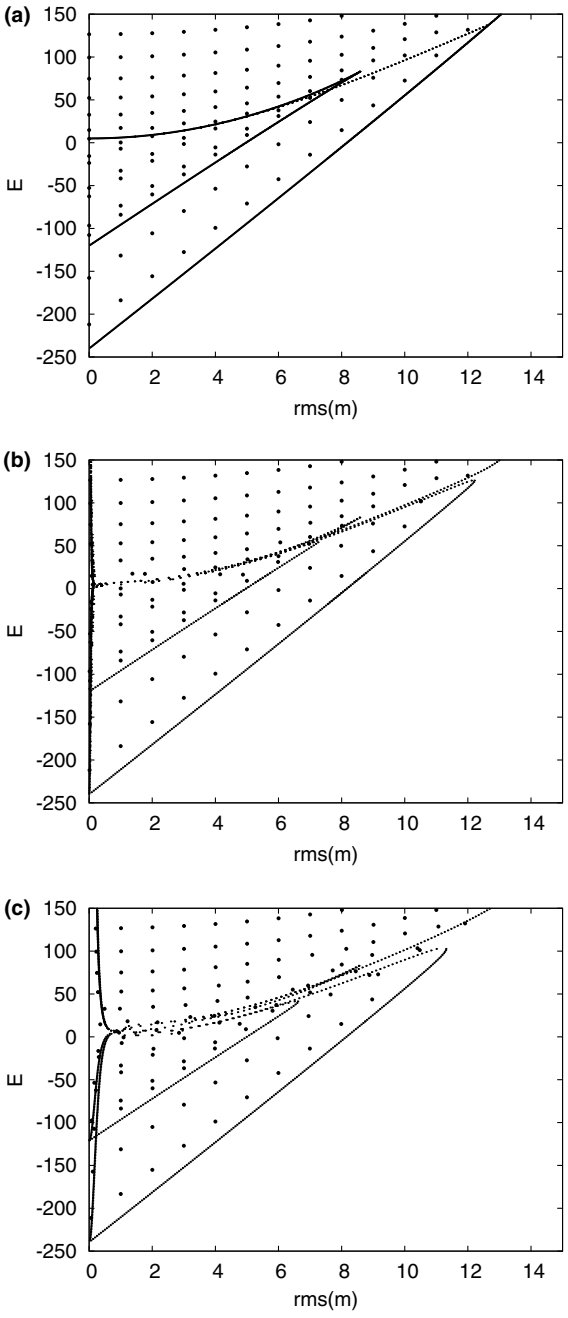

Fig. 4. (a) Collinear fields, integrable case: tilt angle $\beta = 0$, $\omega = 60$, $\Delta\omega = 180$. Classical E versus $|m|$ plots for relative equilibria (solid lines) and resonant periodic orbits (dotted line) are shown together with the quantum $\langle\hat{H}\rangle$:$\sqrt{\langle m^2\rangle}$ lattice (filled circles) for positive parity eigenstates. $|m|$ is a constant of the motion. (b) Tilted fields, nonintegrable case: tilt angle $\beta = \pi/100$, $\omega = 60$, $\Delta\omega = 180$. Classical E versus $\sqrt{m^2}$ plots for primary periodic orbits (dotted lines) together with quantum $\langle\hat{H}\rangle$:$\sqrt{\langle m^2\rangle}$ lattice for positive parity eigenstates. (c) As for (b), tilt angle $\beta = \pi/20$.

A corresponding plot for the $\beta = \pi/20$ case is shown in Fig. 4c. The disruption of the lattice is more severe in this case. It is also numerically more difficult to find classical periodic orbits near $\theta \sim 0, \pi$.

5. Summary and conclusion

We have investigated the classical and quantum mechanics of a diatomic molecule in combined electrostatic and pulsed laser fields. For the integrable case of collinear fields, the system exhibits quantum monodromy, and we have computed classical and quantum energy–momentum (E:m) diagrams for several physically attainable field combinations. The diatomic in a static field perpendicular to the polarization plane of a circularly polarized laser field also exhibits monodromy, and we have verified that the quantum monodromy matrix differs from that for the spherical pendulum case.

For the case of tilted fields, the classical problem is nonintegrable and m is no longer a constant of the motion. For small tilting angles, the lattice obtained by plotting quantum expectation values $\langle\hat{H}\rangle$:$\sqrt{\langle m^2\rangle}$ for eigenstates was nevertheless shown to retain much of the structure of the integrable E:m quantum state lattice, and the corresponding E versus $\overline{m^2}$ curves associated with classical primary periodic orbits were shown to organize the nonintegrable quantum lattice plot. The regular structure of the quantum lattice in the integrable limit was found to be disrupted in an energy range associated with the onset of chaotic classical motion.

References

[1] R.H. Cushman, L.M. Bates, Global Aspects of Classically Integrable Systems, Birkhauser, Basel, 1997.
[2] P.H. Richter, H.R. Dullin, H. Waalkens, J. Wiersig, J. Phys. Chem. 100 (1996) 19124.
[3] J.J. Duistermaat, Comm. Pure Appl. Math. 33 (1980) 687.
[4] R. Cushman, J.J. Duistermaat, Bull. Am. Math. Soc. 19 (1988) 475.
[5] D. Sadovskii, B.I. Zhilinskii, Phys. Lett. A 256 (1999) 235.
[6] M.S. Child, T. Weston, J. Tennyson, Mol. Phys. 96 (1999) 371.
[7] M.S. Child, J. Phys. A 31 (1998) 657.
[8] R.H. Cushman, D.A. Sadovskii, Europhys. Lett. 47 (1999) 1.
[9] M.P. Jacobson, M.S. Child, J. Chem. Phys. 114 (2001) 262.
[10] M. Joyeux, D.A. Sadovskii, J. Tennyson, Chem. Phys. Lett. 382 (2003) 439.
[11] K. Efstathiou, M. Joyeux, D.A. Sadovskii, Phys. Rev. A 69 (2004), Art. No. 032504.
[12] I.N. Kozin, R.M. Roberts, J. Chem. Phys. 118 (2003) 10523.
[13] B. Friedrich, D.R. Herschbach, Nature 353 (1991) 412.
[14] J.M. Rost, J.C. Griffin, B. Friedrich, D.R. Herschbach, Phys. Rev. Lett. 68 (1992) 1299.
[15] B. Friedrich, D. Herschbach, Int. Rev. Phys. Chem. 15 (1996) 325.
[16] J. Bulthuis, J. Moller, H. Loesch, J. Phys. Chem. A 101 (1997) 7684.
[17] B. Friedrich, D. Herschbach, J. Chem. Phys. 111 (1999) 6157.
[18] B. Friedrich, D. Herschbach, J. Phys. Chem. A 103 (1999) 10280.
[19] B. Friedrich, D. Herschbach, J. Phys. Chem. 99 (1995) 15686.
[20] J.J. Larsen, H. Sakai, C.P. Safvan, I. Wendt-Larsen, H. Stapelfeldt, J. Chem. Phys. 111 (1999) 7774.
[21] L. Cai, J. Marango, B. Friedrich, Phys. Rev. Lett. 86 (2001) 775.
[22] L. Cai, B. Friedrich, in: A.D. Bandrauk, Y. Fujimura, R.J. Gordon (Eds.), Laser Control and Manipulations of Molecules, ACS, Washington, DC, 2002, p. 286.

[23] H. Stapelfeldt, T. Seideman, Rev. Mod. Phys. 75 (2003) 543.
[24] H. Sakai, S. Minemoto, H. Nanjo, H. Tanji, T. Suzuki, Phys. Rev. Lett. 90 (2003), Art. No. 083001.
[25] S. Minemoto, H. Nanjo, H. Tanji, T. Suzuki, H. Sakai, J. Chem. Phys. 118 (2003) 4052.
[26] V.I. Arnold, V.V. Kozlov, A.I. Neishtadt, Mathematical Aspects of Classical and Celestial Mechanics, Springer, New York, 1988.
[27] J.A. Montaldi, R.M. Roberts, J. Nonlinear Sci. 9 (1999) 53.
[28] C.A. Arango, W.W. Kennerly, G.S. Ezra (work in progress).
[29] M.C. Gutzwiller, Chaos in Classical and Quantum Mechanics, Springer-Verlag, New York, 1990.
[30] P.B. Corkum, C. Ellert, M. Mehendale, P. Dietrich, S. Hankin, S. Aseyev, D. Rayner, D. Villeneuve, Faraday Discuss. 113 (1999) 47.
[31] J.L. Synge, B.A. Griffith, Principles of Mechanics, third edn., McGraw Hill, New York, 1959.
[32] M. Joyeux, S.C. Farantos, R. Schinke, J. Phys. Chem. A 106 (2002) 5407.
[33] J.M. Greene, R.S. MacKay, F. Vivaldi, M.J. Feigenbaum, Physica D 3 (1981) 468.
[34] R. Cushman, V.N. San, Annal. Henri Poincare 3 (2002) 883.
[35] N. Srivastava, G. Muller, Phys. Lett. A 147 (1990) 282.